Inorganic Chemistry

pubs.acs.org/IC Article

Selective Coordination Mode of Acylthiourea Ligands in Half-Sandwich Ru(II) Complexes and Their Cytotoxic Evaluation

Beatriz N. Cunha,* Liany Luna-Dulcey, Ana M. Plutin, Rafael G. Silveira, João Honorato, Raúl R. Cairo, Tamires D. de Oliveira, Marcia R. Cominetti, Eduardo E. Castellano, and Alzir A. Batista*

Cite This: https://dx.doi.org/10.1021/acs.inorgchem.0c00319 Read Online

ACCESS | Metrics & More | Article Recommendations | Supporting Information

ABSTRACT: In this study, half-sandwich Ru(II) complexes containing acylthiourea ligands of the general type [Ru(η^6-*p*-cymene)(PPh_3)-(S)Cl]PF_6 (**1m**−**6m**) and [Ru(η^6-*p*-cymene)(PPh_3)(S−O)]PF_6 (**1b**−**6b**) where S/S−O = *N*′,*N*′-disubstituted acylthiourea were synthesized and characterized (via elemental analyses, IR spectroscopy, ^{1}H NMR spectroscopy, $^{13}C\{^1H\}$ NMR spectroscopy, and X-ray diffractometry), and their cytotoxic activity was evaluated. The different coordination modes of the acylthiourea ligands, monodentately via S (**1m**−**6m**) and bidentately via S,O (**1b**−**6b**), to ruthenium were modulated from different synthetic routes. The cytotoxicity of the complexes was evaluated in five human cell lines (DU-145, A549, MDA-MB-231, MRC-5, and MCF-10A) by MTT assay. The IC_{50} values for prostate cancer cells (2.89−7.47 μM) indicated that the complexes inhibited cell growth, but that they were less cytotoxic than cisplatin (2.00 μM). Unlike for breast cancer cells (IC_{50} = 0.28−0.74 μM) and lung cancer cells (IC_{50} = 0.51−1.83 μM), the complexes were notably more active than the reference drug, and a remarkable selectivity index (SI 4.66−19.34) was observed for breast cancer cells. Based on both the activity and selectivity, complexes **5b** and **6b**, as well as their respective analogous complexes in the monodentate coordination **5m** and **6m**, were chosen for further investigation in the MDA-MB-231 cell line. These complexes not only induced morphology changes but also were able to inhibit colony formation and migration. In addition, the complexes promoted cell cycle arrest at the sub-G_1 phase inducing apoptosis. Interaction studies by viscosity measurements, gel electrophoresis, and fluorescence spectroscopy indicated that the complexes interact with the DNA minor groove and exhibit an HSA binding affinity.

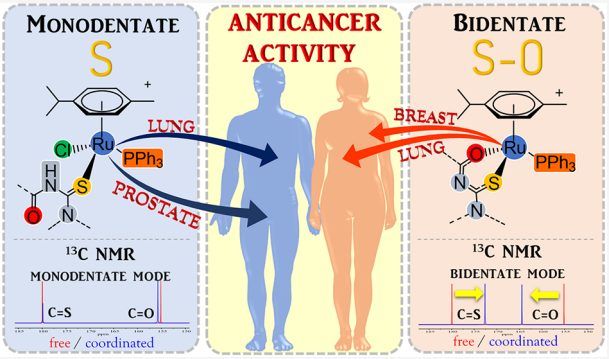

INTRODUCTION

The incidence rate of new cases of cancer has increased significantly worldwide. Breast cancer is the most common cancer for women and is the second leading cause of cancer death among women, while for men, lung and prostate cancers are the main types diagnosed. Considering both sexes, lung, breast, and prostate cancers are responsible for about 33% of the total number of new detected cases.[1] The discovery of cisplatin anticancer properties revolutionized cancer therapy since the approval for the clinical use of cisplatin as a chemotherapeutic agent in 1978, and it is currently widely used.[2,3]

Cisplatin has been used alone or combined with other drugs as a first-line treatment, as an adjuvant, or even as neoadjuvant therapy and is associated with the treatments of bladder, cervical, lung, ovarian, and testicular cancer as well as malignant mesothelioma and squamous carcinoma of the head and neck. In addition, cisplatin is also related to the treatment of other types of cancers where the first-line treatment failed, or in specific situations that preclude the standard treatment.[4] It is estimated that 50% of all cancer patients use cisplatin in their treatment.[5] However, more and more, cisplatin treatment is becoming limited by the development of tumor cell resistance and its side effects.[6,7]

The discovery of other potential drugs has mobilized the scientific community, and metallodrugs have received special attention.[8,9] After cisplatin, a second generation of platinum drugs, such as carboplatin and oxaliplatin, was approved and many others are in clinical trials, which makes platinum the most investigated metal in the development of new metallodrugs.[10] Nonetheless, the search for less toxic drugs also stimulated investigations focused on other metal centers. Ruthenium complexes have been highlighted mainly due to Ru(III) imidazole and indazole compounds, NAMI-A and

Received: January 31, 2020

Scheme 1. Synthesis of Complexes 1m−6m and 1b−6b with the Respective Acylthiourea Ligands

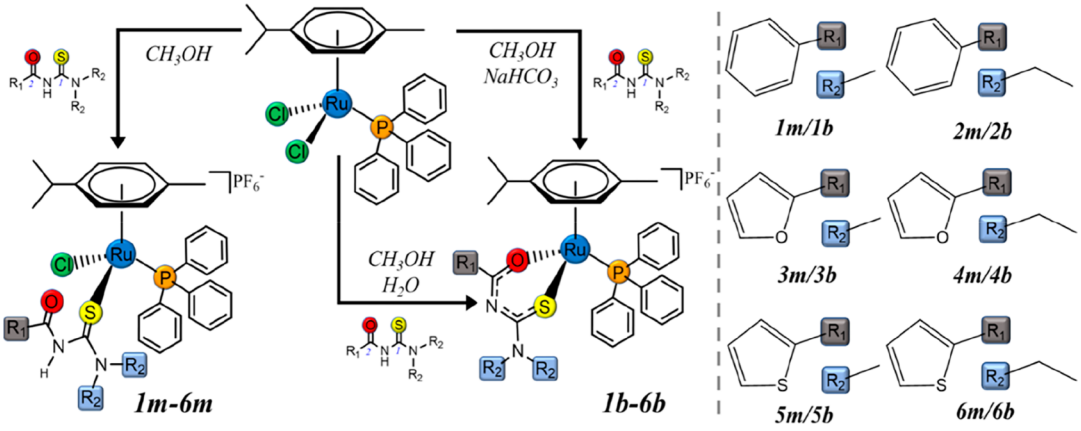

KP1019/KP1339, which showed activities against primary cancer and metastasis.[11,12]

More recently, a new perspective of ruthenium complexes was marked by the investigation of organometallic ruthenium(II)-arene complexes, which were observed mainly in the studies conducted by Dyson and Sadler. In this field, the most promising complexes are [Ru(η^6-*p*-cymene)(PTA)Cl_2] (PTA = 1,3,5-triaza-7-phosphaadamantane), termed RAPTA-C, and [Ru(η^6-*p*-cymene)(en)Cl]$^+$ (en = ethylenediamine). The first is recognized for its activity *in vivo* as an antimetastatic agent, and the second for its cytotoxicity to a range of cancer cell lines, as well as for its metastatic property.[13] Thus, investigations focused on ruthenium(II)-arene complexes with different ligand classes have received great attention in the biological field.[14−17]

Acylthiourea derivatives are established compounds which have been known for more than a century, and their extensive variety of applications makes them interesting molecules.[15] In coordination chemistry, the acylthioureas act as versatile ligands due to the presence of S,N,O donor atoms in their structures, which allows for several coordination modes with different metal centers: (1) O,S bonded to a metal (anionic-bidentate),[18] (2) S bonded to a metal (neutral-monodentate),[19] (3) N bonded to a metal (neutral-monodentate),[20] (4) O,N,N bonded to a metal (anionic-bidentate),[21] (5) O,S bonded to a metal and N bonded to a metal (anionic-briged),[22] and (6) S,N bonded to a metal (anionic-bidentate).[23] The cytotoxicity in the different cell lines of acylthiourea complexes with Ni(II), Co(III), Pd(II), Pt(II), Ru(II), and Au(I) has demonstrated the potential for these compounds as anticancer agents.[24−29]

In the present paper, we focus our study on the investigation of the cytotoxic properties of half-sandwich Ru(II) complexes with acylthioureas acting as monodentate and bidentate ligands. Thus, 12 new complexes of types [Ru(η^6-*p*-cymene)(PPh_3)(S)Cl]PF_6] and [Ru(η^6-*p*-cymene)(PPh_3)(S−O)]PF_6] were obtained, where PPh_3 is triphenylphosphine and S/S−O (**1m** and **1b**) is *N*-(benzoyl)-*N*′,*N*′-dimethyl thiourea, S/S-O (**2m** and **2b**) is *N*-(benzoyl)-*N*′,*N*′-diethyl thiourea, S/S−O (**3m** and **3b**) is *N*-(2-furoyl)-*N*′,*N*′-dimethyl thiourea, S/S−O (**4m** and **4b**) is *N*-(2-furoyl)-*N*′,*N*′-diethyl thiourea, S/S−O (**5m** and **5b**) is *N*-(2-thiophenyl)-*N*′,*N*′-dimethyl thiourea, and S/S−O (**6m** and **6b**) is *N*-(2-thiophenyl)-*N*′,*N*′-diethyl thiourea. The *in vitro* antiproliferative activity of the complexes was evaluated against breast (MDA-MB-231), lung (A549), and prostate (DU-145) human tumor cell lines, as well as breast (MCF-10A) and lung (MRC-5) human non-tumor cell lines. Four selected complexes were investigated not only regarding their effects on cell morphology, colony formation, and migration on MDA-MB-231 but also regarding cell cycle and cellular apoptosis. Additionally, interaction studies with DNA and human serum albumin (HSA) were carried out.

RESULTS AND DISCUSSION

Synthesis and Characterization. The reactions of the precursor complex [Ru(η^6-*p*-cymene)(PPh_3)Cl_2] with *N*-acyl-*N*′,*N*′-disubstituted thiourea produced 12 new complexes with different coordination modes in this ligand class, as can be seen in Scheme 1. By performing the synthesis in methanol only, the monodentate coordination (via the S atom) of acylthiourea to ruthenium is favored (**1m−6m**). However, by adding sodium bicarbonate salt to the reaction medium another coordination mode of the ligand, such as chelate and negatively charged (**1b−6b**), is obtained. Additionally, if the reaction is conducted in a methanol/H_2O (1:1) mixture the bidentate complexes are also formed (**1b−6b**). For the latter, such an effect is possible due to the hydrolysis of complexes **1m−6m** as reported in our previous study, where similar behavior was observed for the ruthenium complexes with monosubstituted acylthioureas.[30] All complexes were isolated as hexafluorophosphate salts of the type 1:1 electrolytes, as supported by molar conductance, whose measurements were carried out in acetone (128.7−139.8 S cm^2 mol^{-1}).

The single crystal structures of the complexes were obtained by ether diffusion into an acetone solution of complexes **1m−6m** and by the slow evaporation of a dichlomethane/methanol solution for complexes **1b, 2b**, and **4b−6b**. The coordination of the acylthiourea ligands to the metal, monodentate via the S atom (**1m−6m**) and bidentate via the S,O atoms (**1b−6b**), was unambiguously confirmed by X-ray techniques. Crystal data are shown in the Supporting Information (Tables S1−S3). The selected bond distances and angles are summarized in Table 1 as well as in Tables S4 and S5. All of the crystallized complexes present a half-sandwich three-legged "piano-stool" structure in which the ruthenium center has a pseudo-octahedral geometry, as can be seen in Figure 1 and Figure S39. The six carbon atoms of the η^6-*p*-cymene ligand form the seat, while the legs of the "piano-stool" structure are constituted by phosphorus (triphenylphosphine), sulfur (acylthiourea), and chlorine atoms (**1m−6m**) or phosphorus (triphenylphosphine), sulfur, and oxygen (acylthiourea) atoms

https://dx.doi.org/10.1021/acs.inorgchem.0c00319
Inorg. Chem. XXXX, XXX, XXX−XXX

Table 1. Selected Interatomic Distances and Bond Angles for Complexes 5m, 6m, 5b, and 6b

	bond lengths (Å)			
	5m	**6m**	**5b**	**6b**
Ru−P	2.3799(11)	2.3799(15)	2.3670(12)	2.3459(13)
Ru−S	2.3843(11)	2.3696(15)	2.3564(13)	2.3507(13)
Ru−Cl	2.4201(11)	2.4208(16)		
Ru−O			2.073(3)	2.091(4)
S(1)−C(1)	1.698(4)	1.709(6)	1.716(5)	1.720(5)
O(1)−C(2)	1.217(6)	1.204(8)	1.276(6)	1.269(7)
N(1)−C(1)	1.392(6)	1.388(8)	1.347(6)	1.345(7)
N(2)−C(1)	1.303(6)	1.307(8)	1.324(7)	1.345(7)
N(1)−C(2)	1.382(6)	1.398(8)	1.313(7)	1.320(7)
	bond angles (deg)			
	5m	**6m**	**5b**	**6b**
P−Ru−Cl	92.42(4)	91.36(6)		
S−Ru−Cl	90.51(4)	91.18(6)		
S−Ru−P	82.77(4)	82.81(5)	88.36(5)	87.05(5)
S−Ru−O			89.21(10)	89.14(11)
P−Ru−O			87.49(10)	88.67(11)

(**1b**−**6b**), as confirmed by bond angles of S(1)−Ru−Cl, S(1)−Ru−P, P−Ru−Cl, S(1)−Ru−O(1), and O(1)−Ru−P around 90°.

The crystal structures of the five free ligands **1**,[31] **2** (CCDC 14315), **3**,[32] **4**,[33] and **5** (CCDC 1029544) were previously published. The average bond lengths of the thiocarbonyl group (S(1)−C(1) = 1.697−1.709 Å) in complexes **1m**−**6m** are longer than the respective bond lengths of the free ligand (S−C = 1.666−1.688 Å), but the double-bond character is maintained; C═O and all C−N bond lengths remained practically unchanged. In the bidentate coordination (**1b**−**6b**), both thiocarbonyl and carbonyl bond lengths are longer than the corresponding free ligand as well as the analogous monodentate complexes, but the C−N distances (C(1)−N(1) = 1.341−1.357 Å; C(2)—N(2) = 1.308−1.328 Å) are significantly shorter than both the free ligands and the monodentate complexes. The length of C−S, C−O, and C−N in the thiocarbonyl fragment (SCNCO) is between a double and single bond, showing evidence of the existence of π-electron delocalization in a six-membered chelate ring formed upon the bidentate coordination of acylthiourea.[34]

Acylthiourea molecules can assume different conformations, the most commonly known of which are *S*, *M*, *Z*, and *U*, where these letters refer to the position of the C═O and C═S bonds in relation to the central N−H bond.[35] In our case, upon coordination the acylthiourea moiety assumed different conformations, as shown in Figure 1. In the monodentate complexes (**1m**−**6m**), the acylthioureas adopted a nonplanar distorted *S*-shaped conformation where the C═O and C═S groups are located at opposite positions, favoring this coordination mode. On the other hand, for the bidentate complexes (**1b**, **2b**, and **4b**−**6b**) the *U* conformation was observed, in which it plays an important role in the π-electron delocalization for the bidentate S,O coordination mode of the acylthiourea.

Complexes **1m**−**6m** exhibit a band in their IR spectra ranging from 3194 to 3116 cm^{-1}, assigned as N—H stretching vibrations, which is also present in the spectra of free acylthiourea. However, upon coordination to the metal this band was shifted to lower frequencies, showing evidence that the coordinate form of the ligand is protonated. As expected, this band is not observed for complexes **1b**−**6b**, which indicates the anionic nature of acylthiourea upon coordination to metal. The νC═O, around 1680 cm^{-1}, in complexes **1m**−**6m** did not change significantly when compared with the free ligand. On the other hand, for complexes **1m**−**6m** the νC═O showed a significant displacement to negative regions, by around 90−183 cm^{-1}, as expected for the S,O coordination mode of the ligands.[24] For all complexes, the νC═S band, at around 1260 cm^{-1}, shifted for lower energy regions due to the weakening of the C═S bond upon coordination of the ligand to the ruthenium metal. An intense band near 840 cm^{-1} in the complexes refers to νP−F and shows evidence of the presence of PF_6^-, as supported by the molar conductance values. Weak vibrations were observed at around 495−501 cm^{-1} and around 336−377 cm^{-1}, which are characteristic of Ru−S and Ru−O stretching, respectively. For complexes **1m**−**6m**, only the νRu−S was observed due to the monodentate coordination of

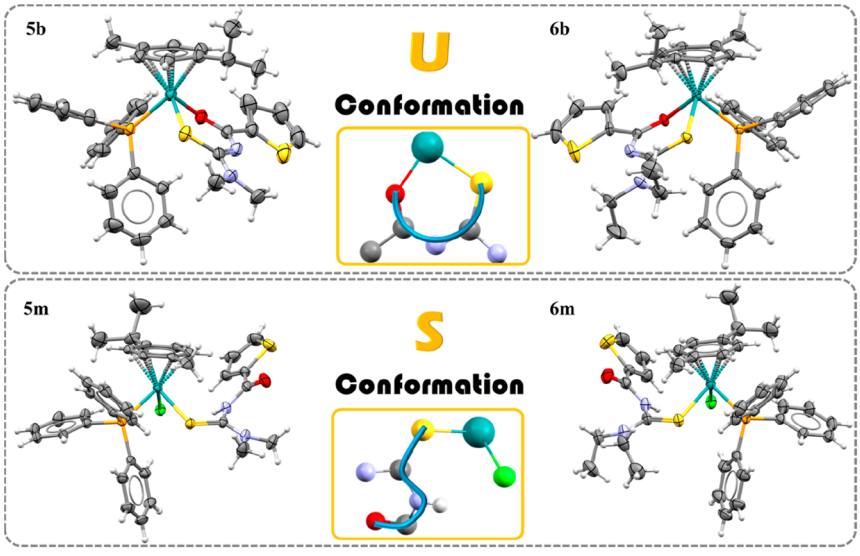

Figure 1. Crystal structures of complexes **5m**, **6m**, **5b**, and **6b**. For the sake of clarity, the PF_6^- counterions are not included.

https://dx.doi.org/10.1021/acs.inorgchem.0c00319
Inorg. Chem. XXXX, XXX, XXX−XXX

Table 2. Characteristic $^{13}C\{^{1}H\}$ NMR Signals in Experimental and Theoretical Data (ppm) For Acylthiourea Ligands and Complexes

^{13}C NMR experimental						^{13}C NMR theoretical					
	Ligands			Complexes			Ligands			Complexes	
	C=O	C=S		C=O	C=S		C=O	C=S		C=O	C=S
1	164.5	181.6	1m	165.2	181.0	**1**	163.7	179.4	**1m**	164.6	178.2
			1b	172.4	174.9				**1b**	164.8	167.6
2	164.9	181.2	2m	165.7	180.7	**2**	164.0	177.8	**2m**	166.0	177.0
			2b	171.7	173.7				**2b**	168.0	169.2
3	154.6	180.5	3m	155.1	180.1	**3**	155.7	185.4	**3m**	152.8	176.3
			3b	164.1	174.0				**3b**	156.6	167.6
4	155.1	180.0	4m	155.8	179.8	**4**	153.1	177.3	**4m**	152.9	175.0
			4b	164.4	172.6				**4b**	158.7	168.9
5	159.0	181.0	5m	159.6	180.3	**5**	157.8	178.6	**5m**	156.8	177.1
			5b	168.0	173.5				**5b**	159.0	166.5
6	159.4	180.5	6m	160.1	180.0	**6**	158.7	178.5	**6m**	157.2	177.2
			6b	168.3	172.5				**6b**	161.0	162.4

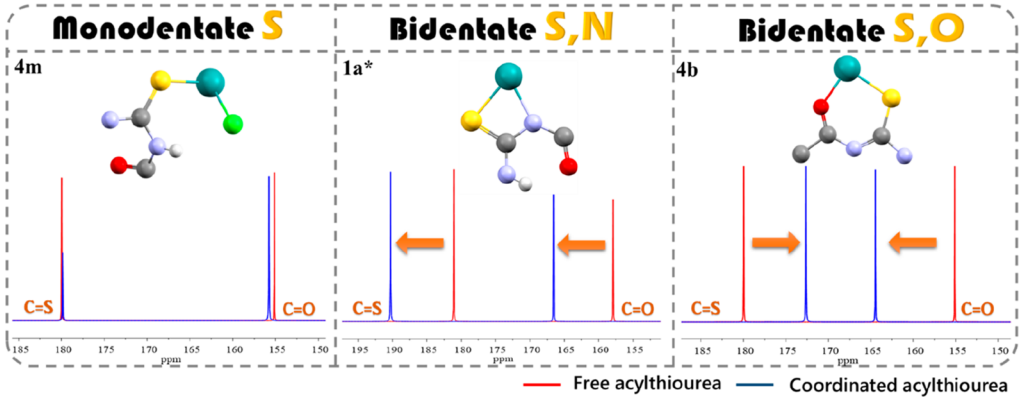

Figure 2. $^{13}C\{^{1}H\}$ NMR spectra of complexes **4m**, **4b**, and **1a** (* reported early)[29] and the respective free ligands in acetone-d_6.

the acylthiourea ligand, while for the bidentate form (**1b**−**6b**), both νRu−S and νRu−O were present.

All complexes were characterized by not only multinuclear $^{31}P\{^{1}H\}$, ^{1}H, and $^{13}C\{^{1}H\}$ NMR experiments but also two-dimensional correlation spectroscopy, COSY, HSQC, and HMBC for the correct assignment of signals (Figures S1−S38). With regard to ^{1}H and $^{13}C\{^{1}H\}$ NMR spectra, the signals of all synthesized complexes show the expected number of peaks, splitting, and intensities corresponding with *p*-cymene, triphenylphosphine, and acylthiourea ligands in a 1:1:1 ratio. In the $^{31}P\{^{1}H\}$ spectra of the complexes, two sets of signals were observed: a singlet for coordinated phosphorus around 28−29 ppm for the **1m**−**6m** complexes and one around 33−35 ppm for the **1b**−**6b** complexes, which shifted to lower frequencies when compared with the precursor (24 ppm) as a consequence of the Cl^{-} labilization. Another set refers to a septet signal of the PF_6^{-} anion at −144 ppm.

In the ^{1}H NMR spectra of the free acylthiourea ligands there is a singlet referring to the N−H hydrogen in the range of 9.19−9.65 ppm. For complexes **1m**−**6m**, this signal was shifted to 11.05−11.37 ppm due to the proximity of N−H to the coordination center, but for complexes **1b**−**6b** the N−H hydrogen is absent. This result confirms the neutral and anionic forms of the acylthiourea ligands upon their coordination to the metal center for the monodentate and bidentate complexes, respectively, as supported by the IR technique. Complexes **1m**−**6m** and **1b**−**6b** showed different behaviors in their $^{13}C\{^{1}H\}$ NMR spectra, mainly in the C=O and C=S carbon signals, when compared with the free ligands, as shown in Table 2. For complexes **1m**−**6m**, these signals did not change significantly, shifting less than 1 ppm for higher and lower frequencies. Complexes **1b**−**6b** presented the same trend, but prominent shifts were observed, close to 9 and 8 ppm for C=O and C=S carbon signals, respectively.

These results are in agreement with the literature, where for the monodentate (S) coordination of acylthiourea to different metal centers the C=O and C=S carbon signals remain virtually unchanged.[36−38] In the bidentate (S,O) coordination mode, a considerable displacement is observed, around 10 ppm, for higher and lower frequencies in relation to the C=S and C=O carbon signals of free acylthiourea, respectively.[39−41] This considerable displacement is due to the π-electron delocalization of the chelate ring formed upon coordination of the acylthiourea molecule to the metal center, as also supported by X-ray diffraction.

Additionally, for an unusual coordination mode of the acylthiourea ligand to the metal (bidentate through the S,N amidic), both the C=S and C=O signals are shifted to lower frequencies by around 9 ppm compared to the free ligand,[20,30] suggesting that in this case there is not a resonance of the π-electrons in the four-member chelate. The same trend was observed regarding the shifts of the C=S and C=O signals in the $^{13}C\{^{1}H\}$ NMR from theoretical data obtained by density functional theory (DFT), which are in good agreement with

https://dx.doi.org/10.1021/acs.inorgchem.0c00319
Inorg. Chem. XXXX, XXX, XXX−XXX

Table 3. IC_{50} Values Obtained from *in Vitro* Cytotoxic Assays against DU-145, A549, MDA-MB-231, and MCF-10A Cell Lines with 48 h of Incubation for the Complexes Compared with the Reference Drug (Cisplatin), Precursor, and Acylthiourea Ligands

	$IC_{50} \pm SD$ (μM)						
complex	DU-145	A549	MDA-MB-231	MRC-5	MCF-10A	SI^{1a}	SI^{2b}
1m	5.60 ± 0.33	1.39 ± 0.22	0.73 ± 0.07	1.61 ± 0.54	4.25 ± 0.55	1.16	5.82
2m	3.87 ± 0.09	0.62 ± 0.12	0.74 ± 0.02	0.94 ± 0.05	3.45 ± 0.22	1.52	4.66
3m	6.01 ± 0.26	1.83 ± 0.01	0.50 ± 0.02	2.47 ± 0.27	5.72 ± 0.44	1.35	11.44
4m	5.73 ± 0.27	0.69 ± 0.18	0.56 ± 0.03	1.12 ± 0.18	4.55 ± 0.22	1.62	8.12
5m	4.45 ± 0.62	0.71 ± 0.02	0.67 ± 0.09	1.23 ± 0.33	6.67 ± 0.95	1.73	9.95
6m	2.89 ± 0.05	0.51 ± 0.02	0.38 ± 0.05	1.22 ± 0.50	6.61 ± 0.51	2.39	17.39
1b	7.47 ± 0.41	2.41 ± 0.03	0.61 ± 0.13	1.83 ± 0.43	3.14 ± 0.58	0.76	5.15
2b	3.27 ± 0.17	0.87 ± 0.02	0.39 ± 0.18	0.87 ± 0.04	5.50 ± 0.31	1.00	14.10
3b	7.37 ± 0.94	1.41 ± 0.11	0.46 ± 0.08	1.85 ± 0.27	6.17 ± 0.13	1.31	13.41
4b	6.22 ± 0.08	0.56 ± 0.08	0.35 ± 0.09	1.29 ± 0.01	3.46 ± 0.20	2.30	9.89
5b	3.19 ± 0.75	1.32 ± 0.14	0.34 ± 0.05	1.11 ± 0.06	6.19 ± 0.25	0.84	19.34
6b	4.08 ± 0.19	0.59 ± 0.07	0.28 ± 0.02	1.03 ± 0.02	4.26 ± 0.38	1.75	15.21
ligands	>100	>100	>100	>100	>100		
precursor	49.68 ± 1.79	12.73 ± 0.17	21.63 ± 1.31	50.65 ± 0.21	19.09 ± 1.03	3.98	0.88
cisplatin	2.00 ± 0.47	11.84 ± 1.19	2. 44 ± 0.20	29.09 ± 0.78	29.45 ± 0.85	2.46	12.07

[a]$SI^1 = IC_{50}$ MRC-5/IC_{50} A549. [b]$SI^2 = IC_{50}$ MCF-10A/IC_{50} MDA-MB-231.

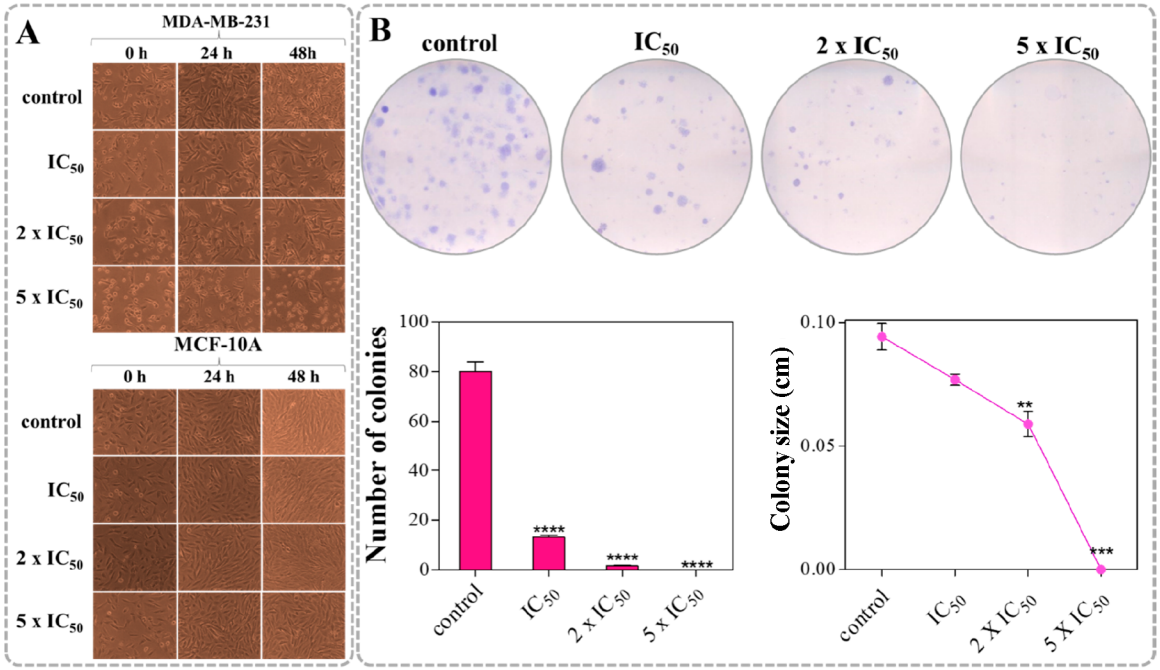

Figure 3. Effects of complex **6b** at IC_{50}, 2 × IC_{50}, and 5 × IC_{50} concentrations in the breast cells. (A) Morphology of MDA-MB-231 and MCF-10A at 0, 24, and 48 h. (B) Colony formation and quantification of colony number and size. Significant at the $^*p < 0.05$, $^{**}p < 0.01$, $^{***}p < 0.001$, and $^{****}p < 0.0001$ levels using ANOVA.

the experimental data for different coordination modes that include the S,N mode, as can be seen in Table 2 and Table S6. Thus, we suggest that the $^{13}C\{^1H\}$ NMR technique may be very useful, not only for allowing the prediction of the coordination mode of the acylthiourea ligands to the ruthenium center but also for the coordination to the other diamagnetic metal center, based only on C═S and C═O carbon shifts of complexes when compared to the free ligand, as shown in Figure 2.

Cytotoxic Activity. The *in vitro* toxicity of the complexes and the free acylthiourea molecules was evaluated against three human tumor cell lines, prostate (DU-145), lung (A549), and breast (MDA-MB-231), and two nontumorigenic human cell lines, lung (MRC-5) and breast (MCF-10A), by colorimetric MTT assay. The IC_{50} values and selective index (SI) are summarized in Table 3. All complexes were significantly more cytotoxic than the respective precursor and acylthiourea ligands for all evaluated cell lines, indicating that the coordination of acylthiourea to the ruthenium enhanced the cytotoxicity of both the precursor and the ligands. Moreover, the antiproliferative activity of the complexes was notably greater than that of the reference drug, cisplatin, in MDA-MB-231 and A549 cells, while for DU-145 cells the complexes were slightly less active than cisplatin.

https://dx.doi.org/10.1021/acs.inorgchem.0c00319
Inorg. Chem. XXXX, XXX, XXX−XXX

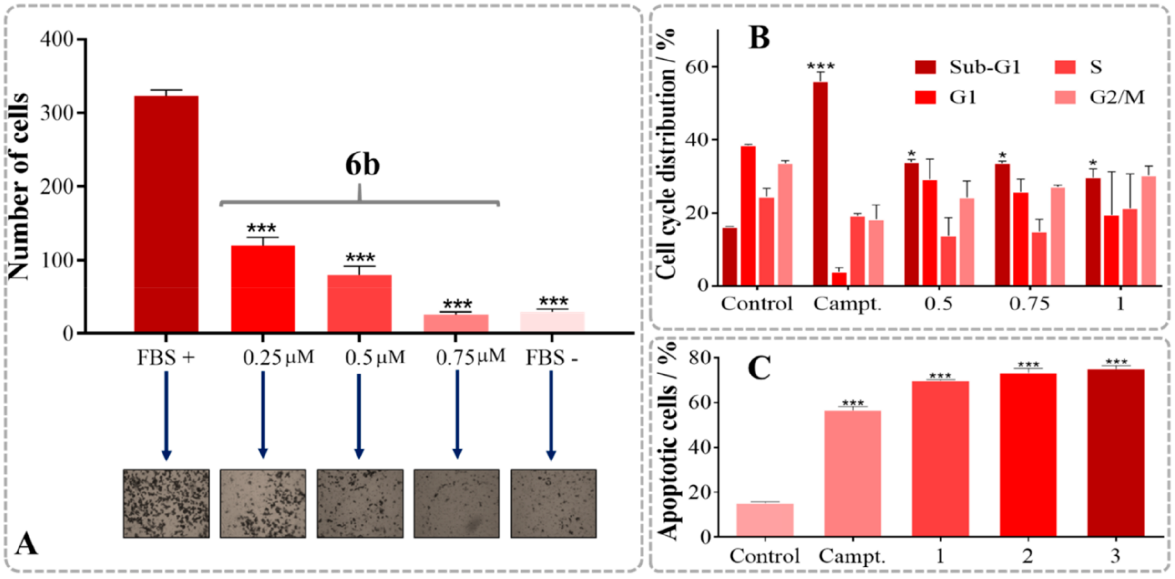

Figure 4. Effects of complexes **5m, 6m, 5b**, and **6b** on MDA-MB-231 cells. (A) Boyden chamber assay of complex **6b** at different concentrations and control with FBS (FBS+) and without FBS (FBS−). Significant at the ***$p < 0.0001$ level using ANOVA. (B) Effects of complex **6b** at different concentrations on cell cycle distribution. (C) Apoptosis by PE-Annexin V with 7-AAD assay. Control corresponds to the untreated cells, and camptothecin was used as a positive control. Significant at the *$p < 0.05$ and ***$p < 0.0001$ levels using ANOVA. Cell cycle distribution.

The therapeutic window was investigated for lung and breast cell lines, where the complexes were more active. The complexes displayed a slight selectivity toward lung cancer cells, showing SI values lower than for the cisplatin. However, for the MDA-MB-231 cell line, the selectivity of all complexes toward cancer cells is clear, with SI around 20 for complexes **5b** and **6b**, which are higher than for cisplatin.

Despite the similar effect of the complexes for specific cell lines, a trend was generally observed: complexes with a monodentate coordination mode of the acylthiourea were more cytotoxic than the analogous complexes in a bidentate form for DU-145 and A549 cells. The opposite occurs for the MDA-MB-231 cell line, where the complexes in bidentate form showed lower IC_{50} values to the detriment of the monodentate complexes. In addition, complexes with an R_1 = thiophene group led to the most cytotoxicity in all studied cancer cell lines. Furthermore, the relationship of the R_2 chain length and activity indicates that the cytotoxicity increases with the chain length of the alkane. In almost all complexes and cell lines, complexes where R_2 = ethyl group were more cytotoxic than the others. Thus, the most active complex for prostate and lung cancer cells was **6m**; for breast cancer cells, complex **6b** was the most active while **6m** was the most selective.

Many publications have shown that increasing the length of the carbon chain increases the lipophilicity of complexes as well as the cytotoxicity.[42,43] It is known that lipophilicity has an influence on the lipid solubility and tissue and cellular uptake.[44] From these results, considering that complexes **5b**, **6b**, **5m**, and **6m** were the most active, with remarkable selectivity on the MDA-MB-231 cell line, they were selected for more detailed biological studies that included an investigation of the mechanism of cell death in this cell line. Therefore, studies were performed with these complexes on cell morphology, clonogenic and antimigration assays, apoptosis analysis, and their interaction with DNA and human serum albumin (HSA).

After exposure of the complexes to breast cancer cells for 24 and 48 h, morphological changes and cell death were observed (Figure 3A and Figures S40−S42). The evaluated complexes showed a similar effect on MDA-MB-231 cells, inducing shrinkage, membrane blebbing, and cell detachment, which are characteristic of apoptotic cell death.[45,46] These effects were intensified when both the concentration of complexes and the time of exposure were increased. For nontumorigenic breast cells, the complexes did not promote considerable morphological changes; only at the highest concentrations studied was a slight inhibition for cell proliferation observed. Thus, the selectivity of the complexes toward cancer cells is clear.

Colony formation is a useful assay in determining the effectiveness of cytotoxic agents based on cell reproduction after treatment with the compound of interest.[47] The complexes, at different concentrations, considerably inhibited the colony formation and colony size in MDA-MB-231 cells when compared with the control (Figure 3B and Figure S43), indicating not only the cytotoxic but also the cytostatic properties of these complexes.

Since migration is an important step of angiogenesis, which is related to tumor metastasis, the ability of the complexes to inhibit the migration cell in the MDA-MB-231 cell line was investigated by both wound healing and Boyden chamber migration assays (Figure 4A and Figures S44−S47). Unlike the control, where the cells spontaneously migrated until complete wound closure, the complexes decreased the migration capacity of breast tumor cells, and the existence of the wound after 24 h of cell treatment with the complexes was observed. This result was also supported by Boyden chamber assay, in which the complexes drastically reduced the migration in a dose-dependent manner. Considering the concentration of 0.75 μM after 24 h, the number of migrated cells corresponded to 25, 60, 79, and 81 for complexes **6b**, **6m**, **5b**, and **5m**, respectively, which are markedly lower values than for the positive control (323 cells), confirming the antimigratory properties of the studied complexes. Despite the fact that complexes **5m**, **6m**, and **5b** showed a similar ability to inhibit the migration, complex **6b** was notably the most inhibitory.

https://dx.doi.org/10.1021/acs.inorgchem.0c00319
Inorg. Chem. XXXX, XXX, XXX−XXX

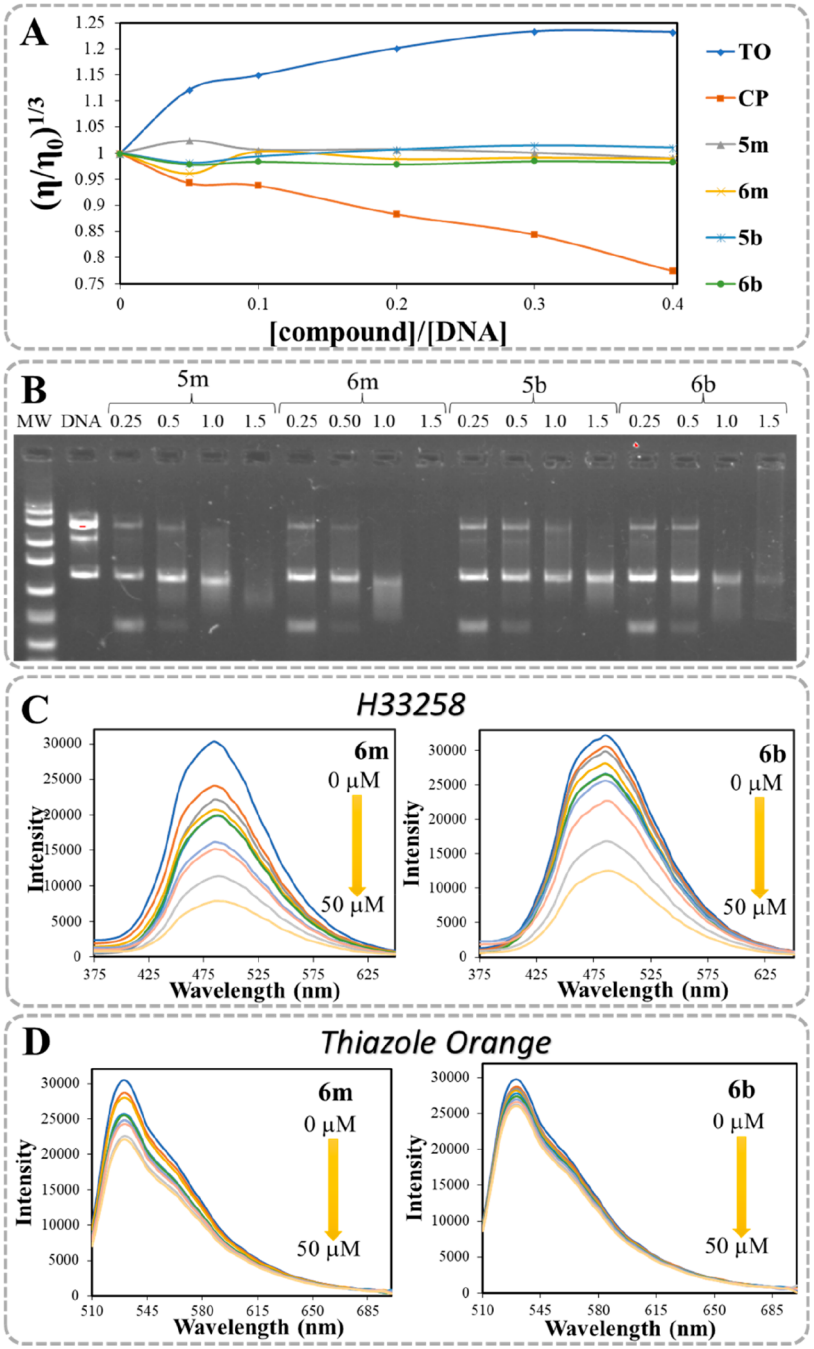

Figure 5. (A) Effects of the concentration of complexes **5m**, **6m**, **5b**, **6b**, thiazole orange (TO), and cisplatin (CP) on the relative viscosity of CT-DNA at 25 °C. (B) Effects of the concentration of complexes **5m**, **6m**, **5b**, and **6b** on the electrophoresis of plasmid pBR322 DNA in different Ri (0.25, 0.5, 1.0, and 1.5), molecular weight marker (MW), and DNA in DMSO (DNA). (C) Emission spectra of Hoechst 33258 (5.0 μM)-CT-DNA (175 μM) (λ_{ex} = 343 nm) at different concentrations (0−50 μM) of complexes **6m** and **6b** at 25 °C. (D) Emission spectra of thiazole orange (5.0 μM)-CT-DNA (175 μM) (λ_{ex} = 480 nm) at different concentrations (0−50 μM) of complexes **6m** and **6b** at 25 °C.

The effects of the complexes on cell cycle regulation in MDA-MB-231 cells were evaluated by propidium iodide staining/flow cytometry. All of the studied complexes had similar behavior on cell cycle progression, promoting a significantly increased accumulation at the sub-G_1 phase cells in a dose-dependent manner, as shown in Figure 4B and Figure S48. However, complex **6b** was the most effective, since it promoted a greater accumulation in the sub-G_1 phase cells in lower concentrations than the other complexes. It is known that an increase in the sub-G_1 portion is associated with apoptosis as a cell death pathway.[45]

In order to confirm that the complexes induce apoptosis in the MDA-MB-231 cells, as indicated by both cell morphology assay and cell cycle analysis, a quantitative analysis was performed by flow cytometry. A marked increase in the apoptotic population (Figure 4C and Figure S49) was observed after treatment with the complexes in a dose-dependent manner. The evaluated complexes similarly induced apoptosis in breast cells, where the percentage of apoptotic cells was nearly 80% following treatment with complexes **5m**, **6m**, and **5b** at 10 μM; in the case of complex **6b**, this percentage was around 70, 73, and 75% at 1, 2, and 3 μM,

https://dx.doi.org/10.1021/acs.inorgchem.0c00319
Inorg. Chem. XXXX, XXX, XXX−XXX

respectively. The degree of apoptosis in the MDA-MB-231 cells induced by complex **6b** was greater and in lower concentrations than those in complexes **5m**, **6m**, and **5b**, which is in agreement with the cytotoxic activity and cell cycle investigation. Commonly, apoptosis is the death mechanism used for Ru(II) arene complexes with anticancer activity, and in many cases it is associated with an increase in the sub-G_1 phase of the cell cycle.[14,15,48,49]

The viscosity experiment has proven to be a useful method for investigating the mode of binding of the complexes to DNA by the relationship between viscosity and DNA fragment lengths.[50] The relative viscosity of DNA did not change significantly when increasing the concentration of the complexes, as seen in Figure 5A. This profile is clearly different from thiazole orange (TO), an intercalating molecule, and cisplatin, a covalent binder, which are used as reference compounds. No changes or less-significant changes in the viscosity of DNA can be indicative of weak interactions or a lack of interaction. Electrostatic and groove binding are recognized as weak interactions where the viscosity of DNA remains unaltered.

The interaction of the complexes with DNA was also investigated by electrophoretic mobility of plasmid pBR322 DNA on agarose in gel after an incubation for 18 h at 37 °C. As shown in Figure 5B, an unusual behavior was observed: with the increase of Ri, there was a decrease in the intensity of all bands. However, this effect was more prominent for the monodentate complexes with R_2 = ethyl; for complexes **5m** and **6m**, no band was visible in Ri = 1.5. In some circumstances, groove binders can replace intercalates with ethidium bromide, a marker used in this assay, resulting in the absence of visible bands.[51]

Based on viscosity and electrophoretic mobility experimental data, the possibility of the interaction of the complexes with the DNA minor groove was investigated by the displacement of the Hoechst 33258 assay. Hoechst is a fluorescent dye, well-known for its ability to bind DNA via the minor groove.[52] Thus, compounds capable of interacting with DNA via the minor groove can replace Hoechst, resulting in the quenching of the fluorescence intensity of the Hoechst-DNA complex. Successive additions of the complexes lead to a reasonable decrease in the fluorescence intensity of the Hoechst-DNA system (Figure 5C and Figure S50). Additionally, a thiazole orange displacement assay was carried out in order to evaluate if the complexes are also able to displace an intercalative compound. This assay was performed in the same conditions evaluated for the Hoechst assay. In the presence of increasing amounts of complexes, a moderate decrease in the fluorescence of the TO-DNA complex was observed (Figure 5D and Figure S50). However, it can be observed that the monodentate complexes (**5m** and **6m**) promoted a greater quenching of fluorescence when compared to the the bidentate complexes (**5b** and **6b**).

This result is in agreement with that observed in the DNA electrophoresis, supporting that the absence of visible bands in the agarose gel was related to the displacement of the DNA intercalator ethidium bromide, which is a strong indicator that the complexes interact with DNA via the minor groove since the quenching of the fluorescence of the TO-DNA system is insignificant when compared with the quenching exhibited for the H33258-DNA system. This kind of interaction has already been reported for other cytotoxic Ru(II) arene complexes.[53,54]

Fluorescence spectroscopy is a widely disseminated method for studying interactions between small molecules and HSA, in which tryptophan is the main residue contributing to the intrinsic fluorescence of this protein (HSA).[55] Under the studied conditions, the complexes were nonfluorescent. As shown in Figure 6 and Figure S51, the fluorescence emission of HSA was quenched regularly with additions of the complexes, which confirms the interaction between the complexes and HSA.

Typically, two mechanisms are associated with fluorescence quenching: static and dynamic, which can be expressed by the Stern−Volmer equation and are distinguished from a depend-

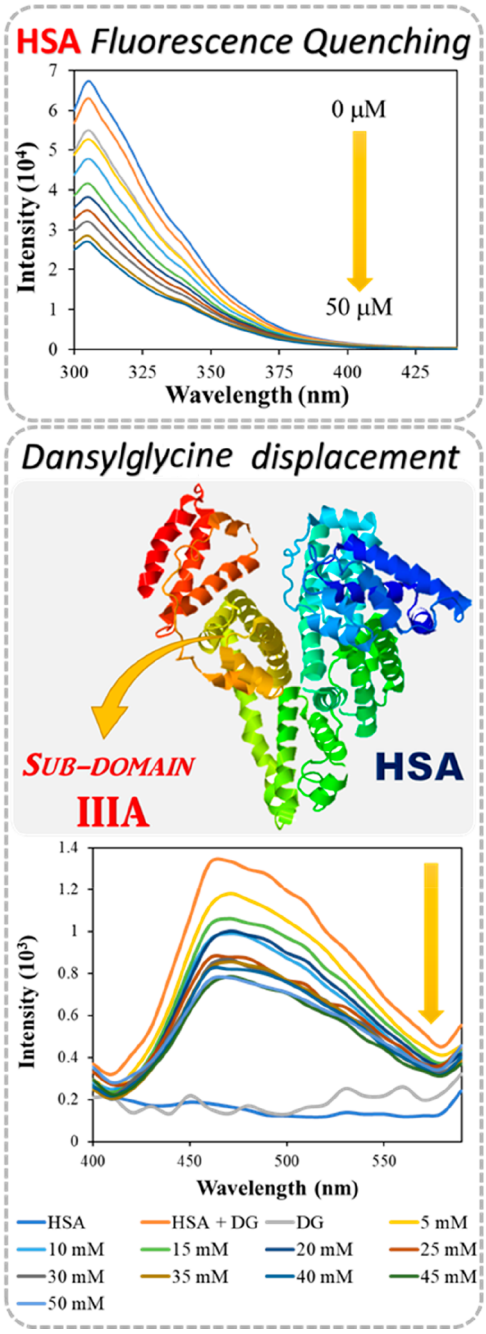

Figure 6. Fluorescence quenching spectra of HSA at different concentrations of complex **6b** at 298 K and fluorescence spectra of HSA-dansylglycine (DG) titrated with complex **6b** at 298 K.

https://dx.doi.org/10.1021/acs.inorgchem.0c00319
Inorg. Chem. XXXX, XXX, XXX−XXX

Table 4. Stern−Volmer Quenching Constants (K_{sv}), Binding Constants (K_b), Numbers of Binding Sites (n), and Thermodynamic Parameters for Ru(II) Complexes at Different Temperatures

	t* (°C)	K_{sv}* (10^4)	K_b* (10^5)	n	$\Delta H°$*	$\Delta S°$*	$\Delta G°$*
5m	298	(4.59 ± 0.09)	(0.40 ± 0.07)	0.96	38.97	218.9	−26.26
	310	(4.30 ± 0.12)	(0.74 ± 0.02)	1.01			−28.89
6m	298	(5.66 ± 0.13)	(0.61 ± 0.03)	1.05	43.68	267.63	−27.28
	310	(5.36 ± 0.13)	(1.19 ± 0.29)	1.1			−36.07
5b	298	(5.15 ± 0.01)	(2.83 ± 0.09)	1.14	139.53	572.58	−31.1
	310	(4.81 ± 0.01)	(25.10 ± 2.25)	1.33			−37.98
6b	298	(6.51 ± 0.07)	(16.27 ± 1.74)	1.31	56.94	308.27	−35.43
	310	(6.21 ± 0.06)	(39.62 ± 1.75)	1.39			−39.15

ence on temperature and viscosity by the Stern−Volmer constant (K_{sv}). For all complexes, K_{sv} values decreased with an increase temperatures (Table 4), indicating a static mechanism, since in the case of the dynamic mechanism the opposite is true and K_{sv} increases with an increase in temperatures.

The binding constant (K_b) values increased with the temperature (Table 4), implying that temperature favors the complex-HSA binding. The K_b values suggest that bidentate complexes (10^5−10^6) exhibit a higher HSA binding affinity than monodentate complexes (10^4−10^5), and complexes with R_1 = ethyl which also showed a higher protein affinity when compared to complexes with R_1 = methyl. Essentially, hydrogen bonds, van der Waals forces, and electrostatic and hydrophobic interactions are involved in protein-molecule binding, and the thermodynamic parameters ($\Delta G°$ = free energy, $\Delta H°$ = enthalpy, and $\Delta S°$ = entropy) can predict the binding mode.[55] As summarized in Table 4, the negative values of $\Delta G°$ for the complexes reveal that the protein binding process is spontaneous. Additionally, both positive $\Delta H°$ and $\Delta S°$ values show evidence of the involvement of hydrophobic forces in the interaction of the complexes with HSA.

The major drug binding sites on HSA are described as sites I and II, which are located in subdomains IIA and IIIA of the protein, respectively. It is established that dansylated amino acids are useful as fluorescent probes in order to distinguish the binging sites.[56,57] In order to indicate the HSA binding site for the complexes, a competitive assay was carried out using dansylglycine (DG) as a marker, since this compound binds to HSA via site II. The HSA-DG complex resulted in increased fluorescence that was blue-shifted (to 470 nm) compared to dansylglycine, as expected. However, a considerable decrease in the fluorescence intensity was observed with successive additions of complexes, as can be seen in Figure 6 and Figure S52. All studied complexes showed similar behavior. This result indicates the affinity of the complexes for the HSA site II.

CONCLUSIONS

Different conditions in the synthetic route modulated distinct coordination modes of acylthiourea ligands in the Ru(II) complexes: monodentately only through S (**1m**−**6m**) and bidentately via S,O (**1b**−**6b**). This ligand class showed different conformations upon coordination, "S" and "U" forms, showing that the type of conformation is associated with specific coordination modes. Interestingly, the $^{13}C\{^1H\}$ NMR technique may be an effective tool to predict the coordination mode among the many possibilities of acylthiourea ligands in different metal centers. Acylthiourea ligand insertion in the half-sandwich Ru(II) complexes contributed considerably to the greater cytotoxicity in breast, lung, and prostate cancer cells. Moreover, this cytotoxicity was significantly higher than cisplatin for breast and lung cancer cells. The structure−activity relation suggested that the complexes, where R_1 = thiophene and R_2 = ethyl, promoted a greater activity in all studied cell lines. In general, monodentate complexes were more cytotoxic in A549 and DU-145 cells, while bidentate complexes were more efficient for MDA-MB-231 cells. Complexes **5m**, **6m**, **5b**, and **6b** inhibit both colony formation and cell migration in breast cancer cells and induce morphological changes. These complexes additionally promote cell cycle arrest at the sub-G_1 phase, and apoptosis cell death. The interaction studies with biomolecules indicate that complexes **5m**, **6m**, **5b**, and **6b** bind to DNA via the minor groove and show a considerable affinity for HSA site II. These results highlight the potential of the half-sandwich Ru(II)/acylthiourea complexes as anticancer agents, encouraging us to explore their chemical properties in more detail in order to better understand this class of compound for greater modulation.

EXPERIMENTAL SECTION

Synthesis of [Ru(η^6-*p*-cymene)(PPh_3)(S)Cl]PF_6 Complexes. The precursors and acylthiourea ligands were synthesized according to previous reports.[32,58−61] The [Ru(η^6-*p*-cymene)(PPh_3)Cl_2] (0.180 mmol, 0.100 g) was dissolved in 20 mL of deaerated methanol, with a subsequent addition of the respective acylthiourea ligand (0.198 mmol). The mixture was kept under an inert atmosphere and was stirred for 0.5 h. Later on, NH_4PF_6 (0.300 mmol, 0.050 g) was added. One hour later, the reaction mixture was concentrated under reduced pressure until the precipitation of an orange solid, which was filtered off, washed with water (3 × 5 mL) and cold methanol (3 × 5 mL), and dried under vacuum.

Synthesis of [Ru(η^6-*p*-cymene)(PPh_3)(S−O)]PF_6 Complexes. The acylthiourea ligand (0.198 mmol) and $NaHCO_3$ (0.198 mmol, 0.017 g) were dissolved in 20 mL of deaerated methanol. Afterward, [Ru(η^6-*p*-cymene)(PPh_3)Cl_2] (0.180 mmol, 0.100 g) was added and the reaction mixture was stirred for 2.5 h under an inert atmosphere. For precipitation of the yellow solid, NH_4PF_6 (0. 300 mmol, 0.050 g) was added. The solid was filtered off, washed with water (3 × 5 mL) and diethyl ether (3 × 5 mL), and dried under vacuum.

These complexes were also obtained by another synthetic route, in which the acylthiourea ligand (0.190 mmol) was dissolved in 20 mL of a deaerated methanolic solution of [Ru(η^6-*p*-cymene)(PPh_3)Cl_2] (0.180 mmol, 0.100 g). After stirring for 0.5 h, under an inert atmosphere, 20 mL of deaerated water was added. The mixture was stirred for 15 h, and the product, which was obtained after the addition of NH_4PF_6 (0. 300 mmol, 0.050 g), was filtered off, washed with water (3 × 5 mL) and diethyl ether (3 × 5 mL), and dried under vacuum.

X-ray Structure Determination. The monodentate complexes were crystallized from a diethyl ether diffusion into an acetone solution of the complexes, while for the bidentate complexes the crystallization occurred by a process of low evaporation of the

https://dx.doi.org/10.1021/acs.inorgchem.0c00319
Inorg. Chem. XXXX, XXX, XXX−XXX

complexes in a dichloromethane/methanol solution. The single crystal measurements by X-ray diffraction were performed on Enraf–Nonius Kappa-CCD and Apex II Duo diffractometers with graphite monochromated MoKα radiation (λ = 0.71073 Å). Cell refinements were carried out using the Collect software,[62] and the structures were obtained by the direct method using SHELXS-97 software.[63] The Gaussian method was used for the absorption corrections.[64] The table and structure representations were generated by WinGX software[65] and MERCURY software,[66] respectively. The main crystal data collections and structure refinement parameters for all complexes are summarized in the Supporting Information.

Theoretical Calculations. The Gaussian 09 revision E.01 electronic structure program suite was used for all DFT calculations.[67] The local density approximation, characterized by the Vosko-Wilk-Nusair (SVWN5) parametrization, was used for the gas phase geometry optimizations.[68] Crystallographic coordinates were used for the optimization (when available) without any restriction of symmetry, and the harmonic frequencies were calculated using the second analytical derivatives and verified for the absence of imaginary frequencies.[69] The ruthenium was described by LANL2DZ relativistic effective core potentials (ECP) that replace 28 core electrons with a nonlocal effective potential and an associated basis set for the remaining electrons, while the 6-31G+(d,p) basis set was used for all other atoms.[70,71] In order to determine the chemical shifts of ^{13}C, the GIAO method was used and the data were compared to the experimental data using eq 1.[72]

$$\delta_{iso,calc} = \sigma_{ref} - \sigma_{iso} \quad (1)$$

where σ_{ref} = 182.4254 ppm was used for ^{13}C (TMS). The TMS crystal structure (CCDC 678366) was optimized at the same level of complex molecule theory.

Cell Culture. MDA-MB-231 (ATCC no. HTB-26) human breast tumor cells, A549 (ATCC no. CCL-185) human lung tumor cells, and MRC-5 (ATCC no.CCL-171) nontumor human lung cells were maintained in a DMEM medium containing 10% fetal bovine serum (FBS). DU-145 (ATCC no. HTB-81) human prostate tumor cells were maintained in an RPMI-1640 medium also supplemented with 10% FBS. The nontumor human breast cell line, MCF-10A (ATCC no. CRL-10317), was cultivated in a DMEM/F12 medium containing 5% horse serum, EGF (0.02 mg/mL), hydrocortisone (0.05 mg/mL), cholera toxin (0.001 mg/mL), insulin (0.01 mg/mL), penicillin (100 IU/mL), streptomycin (100 mg/mL), and L-glutamine (2 mM). All cell lines were maintained at 37 °C in a humidified 5% CO_2 atmosphere.

Proliferation Assay. The effects of the Ru(II) complexes on the viability of cells were determined by colorimetric assay using MTT [3-(4,5-dimethylthiazol-2-yl)-2,5-diphenyltetrazolium bromide]. A density of 1.5 × 10^4 cells/well was seeded in 150 μL of supplemented medium into 96-well plates. After 24 h, the cells were treated with different concentrations of the complexes (dissolved in sterile DMSO) and incubated for 48 h. MTT (1 mg/mL) was added (30 μL/well), and the plates were incubated again for 4 h. After removal of the medium, the formazan crystals were dissolved in isopropanol. The optical density was measured at 540 nm using a 96-well multiscanner autoreader (ELISA).

Cell Morphology. MDA-MB-231 and MCF-10A cells were seeded (1.0 × 10^5 cells/well) in a 12-well plate and incubated in a supplemented medium at 37 °C in 5% CO_2 for 24 h. After treatment of the cells with different concentrations of complexes (dissolved in sterile DMSO, and for the control only sterile DMSO) the cell morphology was examined in an inverted microscope (Nikon, T5100) with 40× magnification.

Colony Formation. MDA-MB-231 cells (300 cells/well) were seeded in a 6-well plate and maintained in a supplemented medium at 37 °C in 5% CO_2 for 24 h. Cells were treated with different concentrations of the complexes for 48 h; for the control, only sterile DMSO (0.5%) was added at same conditions. The medium was replaced by a fresh medium without any complex, and the plates were incubated for 10 days. The cells were washed with PBS, fixed with methanol and acid acetic (3:1) for 5 min, and stained with 5% crystal violet for 30 min. The colonies formed were analyzed in both number and size using ImageJ software.

Migration. Cell migration was investigated by two methods: wound healing and transwell using Boyden chambers. In the wound healing assay, MDA-MB-231 cells (1.5 × 10^5 cells/well) were plated into 12-well plates and incubated properly until the culture reached 100% confluence. Afterward, a scratch was made in the central portion of every well using a micropipette tip. The cells were incubated with the complexes in the corresponding concentration of IC_{50} (48 h) for 24 h. After this time, 40× images were captured with an inverted optical microscope (Nikon, TS100) coupled to a system for image capture in two different fields by well. For the transwell assay, a density of 0.5 × 10^5 cells/well of MDA-MB-231 was incubated with the complexes at different concentrations and seeded on the upper chamber in a DMEM medium without FBS. In the lower chamber, a DMEM medium with 10% FBS was added. The eventual migration process occurred for 22 h at 37 °C in 5% CO_2. Cells that remained in the upper chamber were removed with a cotton swab, and cells that migrated through the upper chamber membrane were fixed with methanol and stained with 1% toluidine blue. Migrated cells were quantified by manual counting.

Cell Cycle Analysis. MDA-MB-231 cells (4 × 10^5 cells/well) were placed in a 6-well plate and incubated with different concentrations of Ru(II) complexes and 32 μM campthothecin (positive control) for 24 h. Afterward, the cells were collected and washed three times with PBS and fixed overnight in 70% ethanol. The cells were washed again with PBS, incubated with RNaseA (0.2 mg/mL) for 30 min at 37 °C, and stained with a hypotonic fluorochrome solution (5 μg/mL PI, 0.1% sodium citrate, and 0.1% Triton-X-100) 1 h before flow-cytometric analysis. Cell cycle phase distribution was analyzed using Cell Quest (BD Biosciences) computer software with an Accuri C6 flow cytometer (BD Biosciences).

Apoptosis Assay. Apoptotic activity of the evaluated complexes on MDA-MB-231 cells was analyzed by flow cytometry using a PE-Annexin-V Apoptosis Detection Kit. The cells (7.0 × 10^4 cells/well) were plated into 12-well plates and after 24 h of incubation at 37 °C were exposed to different concentrations of complexes for 24 h. Treated cells were washed with cold PBS and then resuspended in a 200 μL of binding buffer (10 mM HEPES/NaOH, pH 7.4, 140 mM NaCl, 2.5 mM $CaCl_2$). PE-Annexin V (2.5 mL) and 7-AAD (2.5 mL) were added in each well and incubated for 20 min at room temperature in the dark. Next, 200 μL of binding buffer was added for analysis using an Accuri C6 flow cytometer. The fluorescence was quantified by Cell Quest software (BD Biosciences).

DNA Binding Experiments. DNA interaction studies with the complexes were performed by viscosity, electrophoresis, and fluorescence quenching experiments using calf thymus CT-DNA or plasmid pBR322. The complexes were dissolved in sterile DMSO, and the assays were carried out based on the dilution, with a final concentration of 10% DMSO for all experiments. Viscosity experiments were carried out using the Ostwald viscometer at 25 °C in a thermostatic water bath. The concentration of the CT-DNA solution in a Tris-HCl buffer (5 mM Tris-HCl, 50 mM NaCl, pH 7.2) was fixed (250 μM), while the concentration of the complexes varied from 0 to 100 μM. The flow time was measured using a digital stopwatch. The relative specific viscosity $(\eta/\eta_0)^{1/3}$ values, where η is the relative viscosity of DNA in the presence of the complexes and η_0 is the relative viscosity of DNA, were plotted versus [complex]/[DNA] ratios. Equation 2 was used to determine the relative viscosity of DNA (η_0) values from the flow time of the DNA solution (t) corrected for the flow time of the buffer (t_0).

$$\eta_0 = \frac{t - t_0}{t_0} \quad (2)$$

DNA electrophoresis experiments were performed using agarose gel. Complexes at different ratios between 0.25 and 1.5 were incubated with pBR322 DNA (38 μM) at 37 °C for 18 h. The samples were electrophoresed for 1.5 h at 80 V on 1% agarose gel in a Tris-acetate-EDTA (TAE) buffer (0.45 M Tris-HCl, 0.45 M acetic

https://dx.doi.org/10.1021/acs.inorgchem.0c00319
Inorg. Chem. XXXX, XXX, XXX–XXX

acid, 10 mM EDTA) and stained with ethidium bromide (2 μL/50 mL). After the electrophoretic run, the bands were visualized using a UV-light transilluminator (ChemiDoc equipment).

The Hoechst 33258 and thiazole orange (TO) displacement assay was carried out by the fluorescence quenching experiment with the Hoechst/TO (5.0 μM)-CT DNA (175 μM) complex in buffer (4.5 mM Tris-HCl, 0.5 mM NaOH, 50 mM NaCl) at pH 7.4. The extinction of the emission intensity of the Hoechst CT DNA at 495 nm (excitation wavelength of 343 nm) or of the TO at 530 nm (excitation wavelength of 480 nm) was monitored using the complexes as suppressors at different concentrations (0−50 μM) in DMSO. Fluorescence spectra were recorded in triplicate using an opaque 96-well plate.

HSA Binding Experiments. HSA interaction studies with the complexes were performed by a fluorescence quenching experiment, where the HSA concentration in buffer (4.5 mM Tris-HCl, 0.5 mM NaOH, 50 mM NaCl) at pH 7.4 was kept constant (5 μM), while the concentration of the complexes was increased from 5 to 50 μM. The extinction of the emission intensity of the HSA tryptophan residues at 305 nm (excitation wavelength 270 nm) was monitored at 25 and 37 °C. For data analysis, the classical Stern−Volmer equation was used (eq 3):

$$\frac{F_0}{F} = 1 + K_{qr_o}[Q] = 1 + K_{sv}[Q] \quad (3)$$

where F_0 and F correspond to the fluorescence intensities in the absence and presence of the quencher, respectively; [Q] is the quencher concentration; and K_{sv} is the Stern−Volmer quenching constant.

The binding constant (K_b) as well as the number of binding sites (n) was determined by plotting the double log graph of the fluorescence data using eq 4.

$$\log \frac{F_0 - F}{F} = \log K_b + n \log[Q] \quad (4)$$

The thermodynamic parameters ΔH, ΔS, and ΔG were obtained by eqs 5 and 6

$$\ln \frac{K_2}{K_1} = \left(\frac{1}{T_1} - \frac{1}{T_2}\right)\frac{\Delta H}{R} \quad (5)$$

where K_1 and K_2 are the binding constants at temperatures T_1 and T_2, respectively; R is the gas constant.

$$\Delta G = -RT\ln K = \Delta H - T\Delta S \quad (6)$$

To evaluate the interaction of the complexes with HSA site II, a displacement assay was performed using the compound dansylglycine as a fluorescent probe. The experiments were performed by adding varying amounts of the complexes (0−50 μM, final concentrations) to a mixture of 5 μM HSA and 5 μM dansylglycine in buffer (4.5 mM Tris-HCl, 0.5 mM NaOH, 50 mM NaCl) at pH 7.4. After adding the complexes, the solutions were incubated for 5 min at 25 °C before measurements were taken. The extinction of the emission intensity of the dansylglycine at 470 nm (excitation wavelength 340 nm) was monitored at 25 °C.

■ ASSOCIATED CONTENT

Supporting Information

The Supporting Information is available free of charge at https://pubs.acs.org/doi/10.1021/acs.inorgchem.0c00319.

Measurements and characterization of all complexes (PDF)

Accession Codes

CCDC 1894724−1894734 contain the supplementary crystallographic data for this paper. These data can be obtained free of charge via www.ccdc.cam.ac.uk/data_request/cif, or by emailing data_request@ccdc.cam.ac.uk, or by contacting The Cambridge Crystallographic Data Centre, 12 Union Road, Cambridge CB2 1EZ, UK; fax: +44 1223 336033.

■ AUTHOR INFORMATION

Corresponding Authors

Beatriz N. Cunha − *Departamento de Química, Universidade Federal de São Carlos—UFSCar, 13561-901 São Carlos, SP, Brazil; Instituto Federal Goiano—IFGoiano, 76300-000 Ceres, GO, Brazil;* orcid.org/0000-0003-3079-1854; Email: beatriznc_@hotmail.com

Alzir A. Batista − *Departamento de Química, Universidade Federal de São Carlos—UFSCar, 13561-901 São Carlos, SP, Brazil*; Email: daab@ufscar.br

Authors

Liany Luna-Dulcey − *Departamento de Gerontologia, Universidade Federal de São Carlos—UFSCar, 13561-901 São Carlos, SP, Brazil*

Ana M. Plutin − *Laboratório de Síntesis Orgánica, Facultad de Química, Universidad dela Habana—UH, Habana 10400, Cuba*

Rafael G. Silveira − *Departamento de Química, Universidade Federal de São Carlos—UFSCar, 13561-901 São Carlos, SP, Brazil; Instituto Federal Goiano—IFGoiano, 76300-000 Ceres, GO, Brazil*

João Honorato − *Departamento de Química, Universidade Federal de São Carlos—UFSCar, 13561-901 São Carlos, SP, Brazil;* orcid.org/0000-0002-1127-6083

Raúl R. Cairo − *Laboratório de Síntesis Orgánica, Facultad de Química, Universidad dela Habana—UH, Habana 10400, Cuba*

Tamires D. de Oliveira − *Departamento de Química, Universidade Federal de São Carlos—UFSCar, 13561-901 São Carlos, SP, Brazil*

Marcia R. Cominetti − *Departamento de Gerontologia, Universidade Federal de São Carlos—UFSCar, 13561-901 São Carlos, SP, Brazil;* orcid.org/0000-0001-6385-7392

Eduardo E. Castellano − *Departamento de Física e Informática, Instituto de Física de São Carlos, Universidade de São Paulo—USP, 13560-970 São Carlos, SP, Brazil*

Complete contact information is available at: https://pubs.acs.org/10.1021/acs.inorgchem.0c00319

Notes

The authors declare no competing financial interest.

■ ACKNOWLEDGMENTS

This study was financed in part by the Coordenação de Aperfeiçoamento de Pessoal de Nível Superior - Brazil (CAPES) - Finance Code 001, CNPq, and FAPESP.

■ REFERENCES

(1) Ferlay, J.; Soerjomataram, I.; Dikshit, R.; Eser, S.; Mathers, C.; Rebelo, M.; Parkin, D. M.; Forman, D.; Bray, F. Cancer Incidence and Mortality Worldwide: Sources, Methods and Major Patterns in GLOBOCAN 2012. *Int. J. Cancer* **2015**, *136* (5), E359−86.

(2) Rosenberg, B.; Vancamp, L.; Trosko, J. E.; Mansour, V. H. Platinum Compounds: A New Class of Potent Antitumour Agents. *Nature* **1969**, *222* (5191), 385−386.

(3) Rosenberg, B.; Van Camp, L.; Krigas, T. Inhibition of Cell Division in Escherichia Coli by Electrolysis Products from a Platinum Electrode. *Nature* **1965**, *205* (4972), 698−699.

(4) dos Santos, N. A.; Carvalho Rodrigues, M. A.; Martins, N. M.; dos Santos, A. C. Cisplatin-Induced Nephrotoxicity and Targets of

https://dx.doi.org/10.1021/acs.inorgchem.0c00319
Inorg. Chem. XXXX, XXX, XXX−XXX

Nephroprotection: An Update. *Arch. Toxicol.* **2012**, *86* (8), 1233−1250.
(5) Apps, M. G.; Choi, E. H. Y.; Wheate, N. J. The State-of-Play and Future of Platinum Drugs. *Endocr.-Relat. Cancer* **2015**, *22* (4), R219−R233.
(6) Barragan, F.; Lopez-Senin, P.; Salassa, L.; Betanzos-Lara, S.; Habtemariam, A.; Moreno, V.; Sadler, P. J.; Marchan, V. Photocontrolled DNA Binding of a Receptor-Targeted Organometallic Ruthenium(II) Complex. *J. Am. Chem. Soc.* **2011**, *133* (35), 14098−14108.
(7) Wheate, N. J.; Walker, S.; Craig, G. E.; Oun, R. The Status of Platinum Anticancer Drugs in the Clinic and in Clinical Trials. *Dalt. Trans.* **2010**, *39* (35), 8113.
(8) Mjos, K. D.; Orvig, C. Metallodrugs in Medicinal Inorganic Chemistry. *Chem. Rev.* **2014**, *114* (8), 4540−4563.
(9) Ellahioui, Y.; Prashar, S.; Gómez-Ruiz, S. Anticancer Applications and Recent Investigations of Metallodrugs Based on Gallium, Tin and Titanium. *Inorganics* **2017**, *5* (1), 4.
(10) Ali, I.; Wani, W. A.; Saleem, K.; Haque, A. Platinum Compounds: A Hope for Future Cancer Chemotherapy. *Anti-Cancer Agents Med. Chem.* **2013**, *13* (2), 296−306.
(11) Murray, B. S.; Babak, M. V.; Hartinger, C. G.; Dyson, P. J. The Development of RAPTA Compounds for the Treatment of Tumors. *Coord. Chem. Rev.* **2016**, *306* (P1), 86−114.
(12) Trondl, R.; Heffeter, P.; Kowol, C. R.; Jakupec, M. A.; Berger, W.; Keppler, B. K. NKP-1339, the First Ruthenium-Based Anticancer Drug on the Edge to Clinical Application. *Chem. Sci.* **2014**, *5* (8), 2925−2932.
(13) Leijen, S.; Burgers, S. A.; Baas, P.; Pluim, D.; Tibben, M.; van Werkhoven, E.; Alessio, E.; Sava, G.; Beijnen, J. H.; Schellens, J. H. M. Phase I/II Study with Ruthenium Compound NAMI-A and Gemcitabine in Patients with Non-Small Cell Lung Cancer after First Line Therapy. *Invest. New Drugs* **2015**, *33* (1), 201−214.
(14) Subarkhan, M. K. M.; Ramesh, R. Ruthenium(II) Arene Complexes Containing Benzhydrazone Ligands: Synthesis, Structure and Antiproliferative Activity. *Inorg. Chem. Front.* **2016**, *3* (10), 1245−1255.
(15) Xu, Z.; Kong, D.; He, X.; Guo, L.; Ge, X.; Liu, X.; Zhang, H.; Li, J.; Yang, Y.; Liu, Z. Mitochondria-Targeted Half-Sandwich Ruthenium II Diimine Complexes: Anticancer and Antimetastasis via ROS-Mediated Signalling. *Inorg. Chem. Front.* **2018**, *5* (9), 2100−2105.
(16) Haghdoost, M. M.; Guard, J.; Golbaghi, G.; Castonguay, A. Anticancer Activity and Catalytic Potential of Ruthenium(II)-Arene Complexes with N, O-Donor Ligands. *Inorg. Chem.* **2018**, *57* (13), 7558−7567.
(17) Suss-Fink, G. Arene Ruthenium Complexes as Anticancer Agents. *Dalt. Trans* **2010**, *39* (7), 1673−1688.
(18) Egan, T. J.; Koch, K. R.; Swan, P. L.; Clarkson, C.; Van Schalkwyk, D. A.; Smith, P. J. In Vitro Antimalarial Activity of a Series of Cationic 2,2'-Bipyridyl- and 1,10-Phenanthrolineplatinum(II) Benzoylthiourea Complexes. *J. Med. Chem.* **2004**, *47* (11), 2926−2934.
(19) Schmitt, B.; Gerber, T. I. A.; Hosten, E.; Betz, R. Monomeric/Dimeric Complexes of Fac-[Re(CO)3]+ with Benzoylthiourea Derivatives. *Inorg. Chem. Commun.* **2012**, *24*, 136−139.
(20) Shen, X.; Shi, X.; Kang, B.; Liu, Y.; Tong, Y.; Jiang, H.; Chen, K. Syntheses, Crystal Structures and Properties of Zn(II) and Cd(II) Complexes Derived from N-(o-Nitrophenyl)-N′-(Methoxycarbonyl) Thiourea(H2omt) and 2,2′-Bipyridine(Bpy) or o-Phenanthroline-(Phen). *Polyhedron* **1998**, *17* (23−24), 4049−4058.
(21) Che, D.-J.; Li, G.; Yao, X.-L.; Wu, Q.-J.; Wang, W.-L.; Zhu, Y. Photochemical Generation of a Novel (O, N′, N″) Coordinated Iron(II) Complex [Fe(FT-Py)2] from a Ferrocenoyl-Functionalized Thiourea Ligand: N-Ferrocenylcarbonyl-N′-(2-Pyridyl)Thiourea (HFT-Py): Crystal and Molecular Structures of HFT-Py and [Fe(FT-Py)2]. *J. Organomet. Chem.* **1999**, *584* (1), 190−196.
(22) Kemp, G.; Roodt, A.; Purcell, W.; Koch, K. R. Unprecedented N, S, O Co-Ordination of the Doubly Deprotonated Anion of N-Benzoyl-N′-Phenylthiourea (H2L2) Bridging Two Rhodium(I) Centres: Crystal Structure of the Acetone Solvate of [(PPh3)2(CO)-Rh(μ-L2-KN′⋮O, S)Rh(PPh3)(CO)]. *J. Chem. Soc., Dalton Trans.* **1997**, No. 23, 4481−4484.
(23) Sokolov, F. D.; Zabirov, N. G.; Yamalieva, L. N.; Shtyrlin, V. G.; Garipov, R. R.; Brusko, V. V.; Verat, A. Y.; Baranov, S. V.; Mlynarz, P.; Glowiak, T.; Kozlowski, H. Coordination Diversity of N-Phosphoryl-N′-Phenylthiourea (LH) towards CoII, NiII and PdII Cations: Crystal Structure of ML2-N, S and ML2-O, S Chelates. *Inorg. Chim. Acta* **2006**, *359* (7), 2087−2096.
(24) Yaseen, S.; Rauf, M. K.; Zaib, S.; Badshah, A.; Tahir, M. N.; Ali, M. I.; Imtiaz-ud-Din; Shahid, M.; Iqbal, J. Synthesis, Characterization and Urease Inhibition, in Vitro Anticancer and Antileishmanial Studies of Co(III) Complexes with N, N, N′-Trisubstituted Acylthioureas. *Inorg. Chim. Acta* **2016**, *443*, 69−77.
(25) Selvakumaran, N.; Pratheepkumar, A.; Ng, S. W.; Tiekink, E. R. T.; Karvembu, R. Synthesis, Structural Characterization and Cytotoxicity of Nickel(II) Complexes Containing 3,3-Dialkyl/Aryl-1-Benzoylthiourea Ligands. *Inorg. Chim. Acta* **2013**, *404*, 82−87.
(26) Plutin, A. M.; Mocelo, R.; Alvarez, A.; Ramos, R.; Castellano, E. E.; Cominetti, M. R.; Graminha, A. E.; Ferreira, A. G.; Batista, A. A. On the Cytotoxic Activity of Pd(II) Complexes of N, N-Disubstituted-N'-Acyl Thioureas. *J. Inorg. Biochem.* **2014**, *134*, 76−82.
(27) Colina-Vegas, L.; Luna-Dulcey, L.; Plutin, A. M.; Castellano, E. E.; Cominetti, M. R.; Batista, A. A. Ru(II)-Arene Acylthioureas Complexes: DNA/HSA-Binding, Anti-Migration and Cell Death in a Triple Negative Breast Tumor Cell Line. *Dalt. Trans* **2017**, *46*, 12865−12875.
(28) Kangara, E. F.; Peega, T.; Harmse, L.; van Wyk, J. L.; Levendis, D. C.; Kotzé, I. A. Conformational Analysis and Potential Anticancer Activity of [Pt(Phen)(L1-KS)2] Studied by Single Crystal X-Ray Diffraction and Variable Temperature 1H and 195Pt NMR Spectroscopy. *New J. Chem.* **2019**, *43* (9), 3665−3672.
(29) Molter, A.; Kathrein, S.; Kircher, B.; Mohr, F. Anti-Tumour Active Gold(i), Palladium(Ii) and Ruthenium(Ii) Complexes with Thio- and Selenoureato Ligands: A Comparative Study. *Dalt. Trans* **2018**, *47* (14), 5055−5064.
(30) Cunha, B. N.; Colina-Vegas, L.; Plutín, A. M.; Silveira, R. G.; Honorato, J.; Oliveira, K. M.; Cominetti, M. R.; Ferreira, A. G.; Castellano, E. E.; Batista, A. A. Hydrolysis Reaction Promotes Changes in Coordination Mode of Ru(II)/Acylthiourea Organometallic Complexes with Cytotoxicity against Human Lung Tumor Cell Lines. *J. Inorg. Biochem.* **2018**, *186*, 147−156.
(31) Pérez, H.; Corrêa, R. S.; Plutín, A. M.; Álvarez, A.; Mascarenhas, Y. N -Benzoyl- N ′, N ′-Dimethylthiourea. *Acta Crystallogr., Sect. E: Struct. Rep. Online* **2011**, *67* (3), No. 647.
(32) Cairo, R. R.; Stevens, A. M.; de Oliveira, T. D.; Batista, A. A.; Castellano, E. E.; Duque, J.; Soria, D. B.; Fantoni, A. C.; Correa, R. S.; Erben, M. F. Understanding the Conformational Changes and Molecular Structure of Furoyl Thioureas upon Substitution. *Spectrochim. Acta, Part A* **2017**, *176*, 8−17.
(33) Fraga, A. R. L.; Collins, A.; Forte, G.; Rescifina, A.; Punzo, F. Structures and Properties in Different Media of N, N-(Diethylcarbamothioyl)Furan-2-Carboxamide: A Ionophore for Sensor Membranes. *J. Mol. Struct.* **2009**, *929* (1−3), 174−181.
(34) Weiqun, Z.; Wen, Y.; Liqun, X.; Xianchen, C. N-Benzoyl-N'-Dialkylthiourea Derivatives and Their Co(III) Complexes: Structure, and Antifungal. *J. Inorg. Biochem.* **2005**, *99* (6), 1314−1319.
(35) Saeed, A.; Khurshid, A.; Jasinski, J. P.; Pozzi, C. G.; Fantoni, A. C.; Erben, M. F. Competing Intramolecular NHOC Hydrogen Bonds and Extended Intermolecular Network in 1-(4-Chlorobenzoyl)-3-(2-Methyl-4-Oxopentan-2-Yl) Thiourea Analyzed by Experimental and Theoretical Methods. *Chem. Phys.* **2014**, *431−432*, 39−46.
(36) Sheeba, M. M.; Muthu Tamizh, M.; Farrugia, L. J.; Endo, A.; Karvembu, R. Chiral (H6-p-Cymene)Ruthenium(II) Complexes Containing Monodentate Acylthiourea Ligands for Efficient Asymmetric Transfer Hydrogenation of Ketones. *Organometallics* **2014**, *33* (2), 540−550.

https://dx.doi.org/10.1021/acs.inorgchem.0c00319
Inorg. Chem. XXXX, XXX, XXX−XXX

(37) Jeyalakshmi, K.; Haribabu, J.; Bhuvanesh, N. S.; Karvembu, R. Half-Sandwich RuCl2(Eta(6)-p-Cymene) Core Complexes Containing Sulfur Donor Aroylthiourea Ligands: DNA and Protein Binding, DNA Cleavage and Cytotoxic Studies. *Dalt. Trans* **2016**, *45* (31), 12518−12531.
(38) Singh, D. P.; Pratap, S.; Shukla, M. Solvent Induced Geometry Transformation of Trigonal Planar Cu(I) Complexes of N-((2/4-Methyoxy Carbonyl) Phenyl)-N′-(Ethoxy/Methoxy Carbonyl) Thiocarbamides to Square-Planar Cu(II) Complexes: Synthesis, Spectral, Single Crystal, DFT and in Vitro Cytotoxic. *Inorg. Chim. Acta* **2014**, *423*, 386−396.
(39) Correa, R. S.; de Oliveira, K. M.; Delolo, F. G.; Alvarez, A.; Mocelo, R.; Plutin, A. M.; Cominetti, M. R.; Castellano, E. E.; Batista, A. A. Ru(II)-Based Complexes with N-(Acyl)-N', N'-(Disubstituted)-Thiourea Ligands: Synthesis, Characterization, BSA- and DNA-Binding Studies of New Cytotoxic Agents against Lung and Prostate Tumour Cells. *J. Inorg. Biochem.* **2015**, *150*, 63−71.
(40) Tan, S. S.; Al-Abbasi, A. A.; Mohamed Tahir, M. I.; Kassim, M. B. Synthesis, Structure and Spectroscopic Properties of Cobalt(III) Complexes with 1-Benzoyl-(3,3-Disubstituted)Thiourea. *Polyhedron* **2014**, *68*, 287−294.
(41) Pérez, H.; Corrêa, R. S.; O'Reilly, B.; Plutín, A. M.; Silva, C. C. P.; Mascarenhas, Y. P. Spectroscopic Characterization and Crystal Structure of Cis-Bis(N-(2-Benzoyl)-N′, N′-Diphenylthioureato-k 2O, S)Nickel(II). *J. Struct. Chem.* **2012**, *53* (5), 921−926.
(42) Gramatica, P.; Papa, E.; Luini, M.; Monti, E.; Gariboldi, M. B.; Ravera, M.; Gabano, E.; Gaviglio, L.; Osella, D. Antiproliferative Pt(IV) Complexes: Synthesis, Biological Activity, and Quantitative Structure-Activity Relationship Modeling. *JBIC, J. Biol. Inorg. Chem.* **2010**, *15* (7), 1157−1169.
(43) Cetraz, M.; Sen, V.; Schoch, S.; Streule, K.; Golubev, V.; Hartwig, A.; Köberle, B. Platinum(IV)-Nitroxyl Complexes as Possible Candidates to Circumvent Cisplatin Resistance in RT112 Bladder Cancer Cells. *Arch. Toxicol.* **2017**, *91* (2), 785−797.
(44) Fonteh, P.; Elkhadir, A.; Omondi, B.; Guzei, I.; Darkwa, J.; Meyer, D. Impedance Technology Reveals Correlations between Cytotoxicity and Lipophilicity of Mono and Bimetallic Phosphine Complexes. *BioMetals* **2015**, *28* (4), 653−667.
(45) Huang, X.; Halicka, H. D.; Traganos, F.; Tanaka, T.; Kurose, A.; Darzynkiewicz, Z. Cytometric Assessment of DNA Damage in Relation to Cell Cycle Phase and Apoptosis. *Cell Proliferation* **2005**, *38* (4), 223−243.
(46) Honorato, J.; Colina-Vegas, L.; Correa, R. S.; Guedes, A. P. M.; Miyata, M.; Pavan, F. R.; Ellena, J.; Batista, A. A. Esterification of the Free Carboxylic Group from the Lutidinic Acid Ligand as a Tool to Improve the Cytotoxicity of Ru(II) Complexes. *Inorg. Chem. Front.* **2019**, *6* (2), 376−390.
(47) Franken, N. A. P.; Rodermond, H. M.; Stap, J.; Haveman, J.; van Bree, C. Clonogenic Assay of Cells in Vitro. *Nat. Protoc.* **2006**, *1* (5), 2315−2319.
(48) Mohamed Kasim, M. S.; Sundar, S.; Rengan, R. Synthesis and Structure of New Binuclear Ruthenium(Ii) Arene Benzil Bis-(Benzoylhydrazone) Complexes: Investigation on Antiproliferative Activity and Apoptosis Induction. *Inorg. Chem. Front.* **2018**, *5* (3), 585−596.
(49) Jovanovic, K. K.; Tanic, M.; Ivanovic, I.; Gligorijevic, N.; Dojcinovic, B. P.; Radulovic, S. Cell Cycle, Apoptosis, Cellular Uptake and Whole-Transcriptome Microarray Gene Expression Analysis of HeLa Cells Treated with a Ruthenium(II)-Arene Complex with an Isoquinoline-3-Carboxylic Acid Ligand. *J. Inorg. Biochem.* **2016**, *163*, 362−373.
(50) Wheate, N. J.; Brodie, C. R.; Collins, J. G.; Kemp, S.; Aldrich-Wright, J. R. DNA Intercalators in Cancer Therapy: Organic and Inorganic Drugs and Their Spectroscopic Tools of Analysis. *Mini-Rev. Med. Chem.* **2007**, *7* (6), 627−648.
(51) Indumathy, R.; Radhika, S.; Kanthimathi, M.; Weyhermuller, T.; Unni Nair, B. Cobalt Complexes of Terpyridine Ligand: Crystal Structure and Photocleavage of DNA. *J. Inorg. Biochem.* **2007**, *101* (3), 434−443.
(52) Jalali, F.; Dorraji, P. S. Interaction of Anthelmintic Drug (Thiabendazole) with DNA: Spectroscopic and Molecular Modeling Studies. *Arabian J. Chem.* **2017**, *10*, S3947−S3954.
(53) Wu, Q.; Zheng, K.; Liao, S.; Ding, Y.; Li, Y.; Mei, W. Arene Ruthenium(II) Complexes as Low-Toxicity Inhibitor against the Proliferation, Migration, and Invasion of MDA-MB-231 Cells through Binding and Stabilizingc-MycG-Quadruplex DNA. *Organometallics* **2016**, *35* (3), 317−326.
(54) Zhao, J.; Li, S.; Wang, X.; Xu, G.; Gou, S. Dinuclear Organoruthenium Complexes Exhibiting Antiproliferative Activity through DNA Damage and a Reactive-Oxygen-Species-Mediated Endoplasmic Reticulum Stress Pathway. *Inorg. Chem.* **2019**, *58* (3), 2208−2217.
(55) Lakowicz, J. R. *Principles of Fluorescence Spectroscopy*; Lakowicz, J. R., Ed.; Springer US: Boston, MA, 2006. DOI: 10.1007/978-0-387-46312-4
(56) Sudlow, G.; Birkett, D. J.; Wade, D. N. Further Characterization of Specific Drug Binding Sites on Human Serum Albumin. *Mol. Pharmacol.* **1976**, *12* (6), 1052−1061.
(57) Sudlow, G.; Birkett, D. J.; Wade, D. N. The Characterization of Two Specific Drug Binding Sites on Human Serum Albumin. *Mol. Pharmacol.* **1975**, *11* (6), 824−832.
(58) Robertson, D. R.; Robertson, I. W.; Stephenson, T. A. Ruthenium Complexes Containing Group VB Donor Ligands. *J. Organomet. Chem.* **1980**, *202* (3), 309−318.
(59) Bennett, M. A.; Smith, A. K. Arene Ruthenium(II) Complexes Formed by Dehydrogenation of Cyclohexadienes with Ruthenium-(III) Trichloride. *J. Chem. Soc., Dalton Trans.* **1974**, No. 2, 233.
(60) Saeed, S.; Rashid, N.; Jones, P. G.; Ali, M.; Hussain, R. Synthesis, Characterization and Biological Evaluation of Some Thiourea Derivatives Bearing Benzothiazole Moiety as Potential Antimicrobial and Anticancer Agents. *Eur. J. Med. Chem.* **2010**, *45* (4), 1323−1331.
(61) Plutín, A. M.; Alvarez, A.; Mocelo, R.; Ramos, R.; Castellano, E. E.; da Silva, M. M.; Villarreal, W.; Pavan, F. R.; Meira, C. S.; Filho, J. S. R.; Moreira, D. R. M.; Soares, M. B. P.; Batista, A. A. Palladium(II)/ N, N -Disubstituted- N ′-Acylthioureas Complexes as Anti- Mycobacterium Tuberculosis and Anti- Trypanosoma Cruzi Agents. *Polyhedron* **2017**, *132*, 70−77.
(62) Hooft, R. W. W. *COLLECT Data Collection Software*; Nonius B. V.: Delft, The Netherlands, 1998.
(63) Sheldrick, G. M. A Short History of SHELX. *Acta Crystallogr., Sect. A: Found. Crystallogr.* **2008**, *64*, 112−122.
(64) Coppens, P.; Leiserowitz, L.; Rabinovich, D. Calculation of Absorption Corrections for Camera and Diffractometer Data. *Acta Crystallogr.* **1965**, *18* (6), 1035−1038.
(65) Farrugia, L. J. WinGXsuite for Small-Molecule Single-Crystal Crystallography. *J. Appl. Crystallogr.* **1999**, *32* (4), 837−838.
(66) Macrae, C. F.; Bruno, I. J.; Chisholm, J. A.; Edgington, P. R.; McCabe, P.; Pidcock, E.; Rodriguez-Monge, L.; Taylor, R.; Van De Streek, J.; Wood, P. A. Mercury CSD 2.0- New Features for the Visualization and Investigation of Crystal Structures. *J. Appl. Crystallogr.* **2008**, *41* (2), 466−470.
(67) Frisch, M. J.; Trucks, G. W.; Schlegel, H. B.; Scuseria, G. E.; Robb, M. A.; Cheeseman, J. R.; Scalmani, G.; Barone, V.; Mennucci, B., et al. *Gaussian 09*; Gaussian, Inc.: Wallingford, CT, 2009.
(68) Vosko, S. H.; Wilk, L.; Nusair, M. Accurate Spin-Dependent Electron Liquid Correlation Energies for Local Spin Density Calculations: A Critical Analysis. *Can. J. Phys.* **1980**, *58* (8), 1200−1211.
(69) Foresman, J. B.; Frisch, A. *Exploring Chemistry with Electronic Structure Methods*, 3rd ed.; Gaussian, Inc.: Wallingford, CT, 2015.
(70) Hariharan, P. C.; Pople, J. A. The Influence of Polarization Functions on Molecular Orbital Hydrogenation Energies. *Theor. Chim. Acta* **1973**, *28* (3), 213−222.
(71) Hay, P. J.; Wadt, W. R. Ab Initio Effective Core Potentials for Molecular Calculations. Potentials for the Transition Metal Atoms Sc to Hg. *J. Chem. Phys.* **1985**, *82* (1), 270−283.

https://dx.doi.org/10.1021/acs.inorgchem.0c00319
Inorg. Chem. XXXX, XXX, XXX−XXX

(72) Gowda, V.; Laitinen, R. S.; Telkki, V. V.; Larsson, A. C.; Antzutkin, O. N.; Lantto, P. DFT Calculations in the Assignment of Solid-State NMR and Crystal Structure Elucidation of a Lanthanum-(Iii) Complex with Dithiocarbamate and Phenanthroline. *Dalt. Trans* **2016**, *45* (48), 19473−19484.

https://dx.doi.org/10.1021/acs.inorgchem.0c00319
Inorg. Chem. XXXX, XXX, XXX−XXX